

We are IntechOpen, the world's leading publisher of Open Access books Built by scientists, for scientists

6,900

Open access books available

186,000

International authors and editors

200M

Downloads

Our authors are among the

154

Countries delivered to

TOP 1%

most cited scientists

12.2%

Contributors from top 500 universities



WEB OF SCIENCE™

Selection of our books indexed in the Book Citation Index
in Web of Science™ Core Collection (BKCI)

Interested in publishing with us?
Contact book.department@intechopen.com

Numbers displayed above are based on latest data collected.
For more information visit www.intechopen.com



Fabrication of 3D Micro- and Nano-Structures by Prism-Assisted UV and Holographic Lithography

Guomin Jiang, Kai Shen and Michael R. Wang

Additional information is available at the end of the chapter

<http://dx.doi.org/10.5772/56417>

1. Introduction

Lithography, the fundamental fabrication process of semiconductor devices, is playing a critical role nowadays in the fabrication of micro- and nano-structures especially for the realization of micro-electro-mechanical systems (MEMS), microfluidic devices, photonic crystals, photonic integrated circuits, micro-optics, and plasmonic optoelectronic devices. These devices have various practical applications including optical display, optical memory, optical interconnection for high speed computing systems, photonic planar lightwave circuits, medical fluidic filtering devices, drug delivery devices, solar energy devices, antireflection optical elements, and optical sensors.

Traditional photolithography, laser direct write maskless lithography, and gray-scale lithography are suitable for micro-structural patterning. E-beam lithography, EUV and X-ray lithography employing shorter wavelength beams can help improve pattern resolution for fabrication of finer scale nano-structures. Contact lithography including soft lithography and nano-imprint lithography offers capability of higher resolution nano-structure fabrication. However, most of these existing lithography tools are limited to the fabrication of two-dimensional (2D) micro- and nano-structures. Multilayer 2D patterning using the photo and e-beam lithography tools can yield 3D layered structures. Such fabricated structures due to multilayer lithography, would be very difficult to achieve high resolution layered thickness control and layer to layer alignment for finer resolution 3D micro-structures.

We present herein prism-assisted inclined ultraviolet (UV) lithography and holographic lithography (HL) for the fabrication of three-dimensional (3D) micro- and nano-structures in SU-8 photoresist. For inclined UV lithography, a prism is used as a refractor to deflect the incident UV light and expand the exposure beam angle range in the resist film. The sample internal surface reflection of the exposing UV light can facilitate the fabrication of symmetric

structures. Prism with multidirectional side surfaces can be used to achieve one-step exposure fabrication of multidirectional slanted structures. For holographic lithography, a prism is used to form multi-directional interference beams that greatly simplify the beam splitting and redirecting in conventional HL and at the same time minimize the system vibration sensitivity. The prism-assisted HL is attractive for fast and large area realization of crystal structures, especially quasi-crystal structures. Some practical applications will be discussed.

2. Prism-assisted inclined UV lithography

Inclined UV lithography has recently been used for the fabrication of 3D microstructures (Beuret et al., 1994; Yoon et al., 2006; Han et al., 2004; Campo & Arzt, 2008; Campo & Greiner, 2007). It has demonstrated effective production of various 3D patterns for many practical applications. Two critical problems, namely limited exposure angle and complicated rotation process, have so far restricted the widespread use of the inclined UV lithography in the fabrication of 3D microstructures.

Many devices, such as optical pick-up heads (Huang et al., 2004), embedded waveguide mirrors (Dou et al., 2010), and sharpened microneedles (Han et al., 2007), require microstructures with large side surface angles measured from the normal direction of the resin surface. The widely used negative photoresist SU-8 (refractive index 1.67 at 365 nm) from MicroChem as an example when exposed directly in air, as shown in Fig. 1, the inclined exposure angle in the lithographic resin can in general be easily adjusted by changing the slanted stage angle. However, the refractive beam path bending associated to the large index difference between the air and photoresist has limited the exposure angles in the resin and thus the realization of large angle side surfaces.

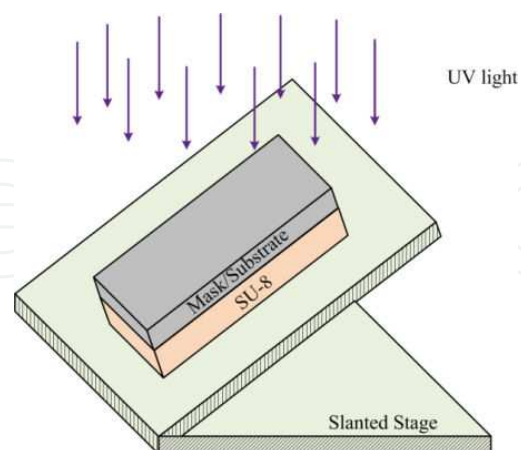


Figure 1. Schematic diagram of inclined UV lithography in the air.

In order to expand the exposure angle in the resin, one way is to immerse the lithographic resin in an index matching liquid (Huang et al., 2004; Han et al., 2007; Ling & Lian, 2007), such as deionized (DI) water ($n=1.33$), heptane ($n=1.39$), or glycerol ($n=1.6$), which can effectively

minimize the light beam path bending, as shown in Fig. 2(a). Fig. 2(b) presents the simulation results of the exposure angle θ in the SU-8 versus slanted stage angle β in air, water, heptane and glycerol, respectively. The exposure angle can be easily increased beyond 45° with the use of an index matching liquid. However, this immersion method demands a sample settlement time in the index matching liquid to avoid uneven liquid surface and bubble formation. The presence of index matching liquid may affect the UV exposure properties of the resin, because of its influence of certain characteristics of the lithographic resin, such as water content.

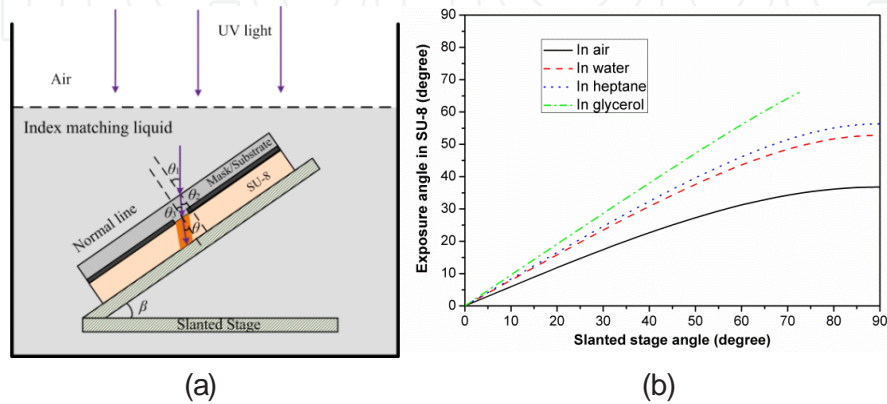


Figure 2. a) Schematic diagram of inclined UV lithography in an index matching liquid and (b) simulation of the exposure angle versus slanted stage angle in air, water, heptane, and glycerol.

Multi-directional inclined structures are normally applied in some more complex devices, such as microfilter and micromixer. Multi-step UV exposure with sample rotation has been proved effective. The slanted sample/mask holder of Fig. 3 can be used for such purpose. It would be more attractive to introduce a one-step fabrication technique for the realization of 3D structures with multi-directional inclined angles.

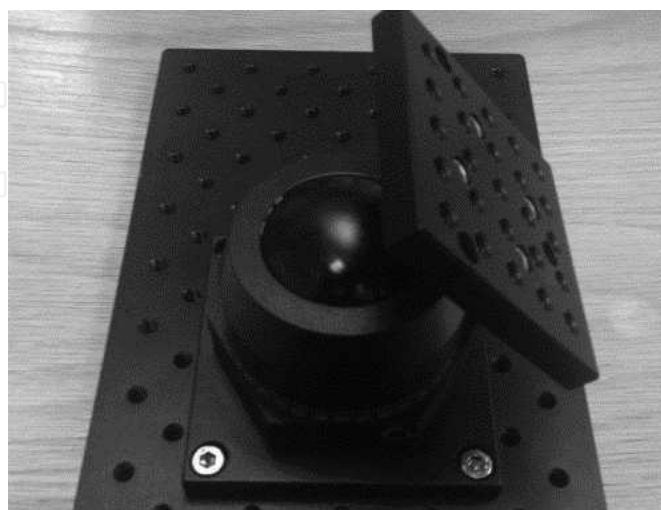


Figure 3. The sample/mask plate holder with rotation features for multi-directional inclined UV exposure.

2.1. Prism-assisted UV lithography for slanted structures with large exposure angles

As schematically presented in Fig. 4, the prism-assisted UV lithography can expand the exposure angle of slanted structures in the resin. A glass prism (refractive index 1.53 at 365 nm) acts as a refractor to deflect the direction of the incident UV light in the resin for the inclined UV lithographic exposure. This overcomes the exposure angle limitation due to the original large index difference between air and photoresist. The back-side UV exposure is applied here for accurate patterning benefiting from the intimate contact between the photomask/substrate and the resin. The prism side surface to bottom surface angle is α . Poly-dimethylsiloxane (PDMS) serves as a good candidate for fast custom prototyping of the prism in house (Kang et al., 2006) with needed prism angle, benefiting from its low cost, molding flexibility, and easy angle control. The slanted stage provides an inclined angle β to the horizontal plane. The incident UV light at 365 nm wavelength is perpendicular to the horizontal plane. In the lithographic exposure process, the refractions of UV light happen at air/prism, prism/mask, and mask/SU-8 interfaces, as schematically illustrated in Fig. 4(b). The relationships between the incident and refractive angles on all interfaces can be obtained based on the Snell's law. The exposure angle θ in SU-8, as a function of the prism angle α and slanted stage angle β , can be written as (Jiang et al., 2012a)

$$\theta = \sin^{-1} \left\{ \frac{n_{prism}}{n_{su-8}} \sin \left[\alpha - \sin^{-1} \left(\frac{n_{air}}{n_{prism}} \sin(\alpha - \beta) \right) \right] \right\},$$

where n denotes the refractive index of each medium.

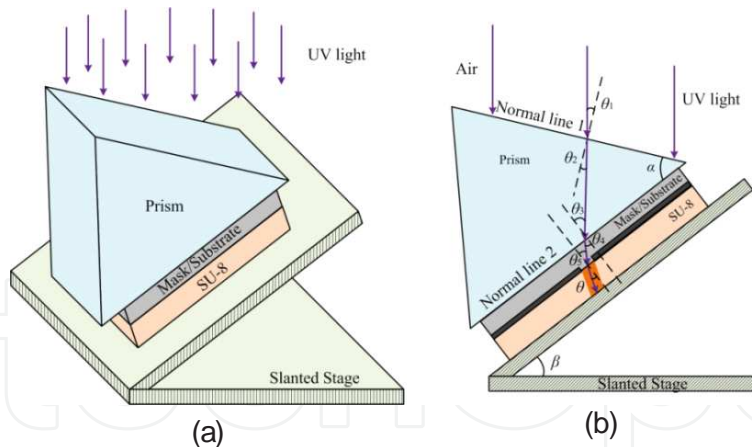


Figure 4. a) Schematic diagram of prism-assisted UV lithography for the expansion of the exposure angle in the resin. (b) Schematic of cross-sectional view of the UV light path bending.

The calculated relationships of exposure angle θ , the prism angle α , and the slanted stage angle β are shown in Fig. 5. The exposure angle in SU-8 can be easily expanded beyond 60° by using this method. Different combinations of α and β to realize 15° (green dash-dot line), 30° (black solid line), 45° (red dotted line), and 60° (blue dashed line) inclined surfaces are also highlighted in this figure. Obviously, we can expand and control the exposure angle in SU-8 by flexibly varying the combination of the prism angle and the slanted stage angle.

Using this technique, we have fabricated 3D slanted structures with different inclined angles of 15° , 30° , 45° , and 60° as illustrated in Fig. 6 (Jiang et al., 2012a). A 45° prism was used in the fabrication process, and the slanted stage angles were set to 0° , 27° , 54° , and 85° , respectively. Some functional and interesting inclined structures with 45° exposure angles (see Fig. 7) can be easily fabricated using this method.

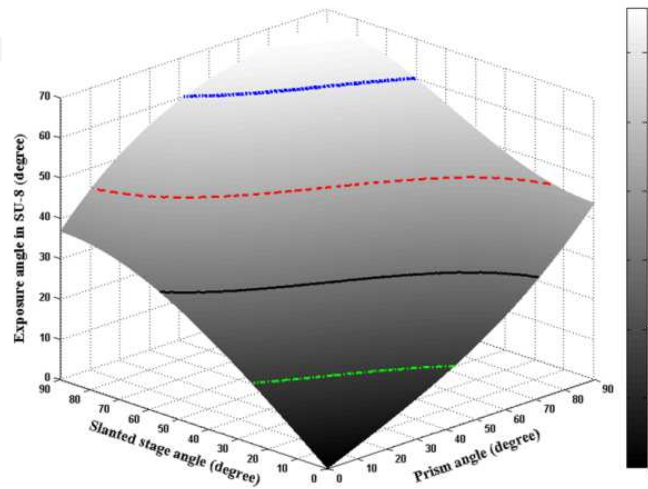


Figure 5. The exposure angle θ in SU-8 as a function of the prism angle α and slanted stage angle β .

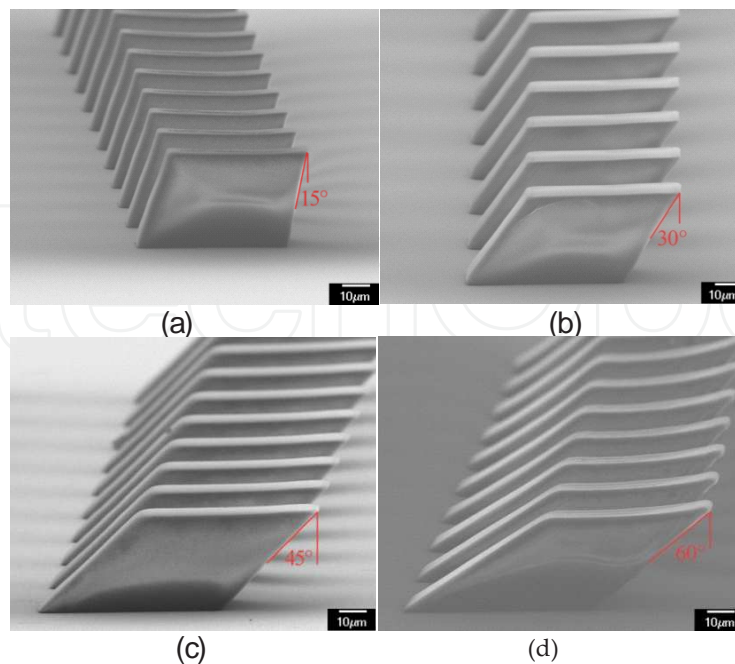


Figure 6. SEM images of the fabricated inclined structures with different exposure angles.

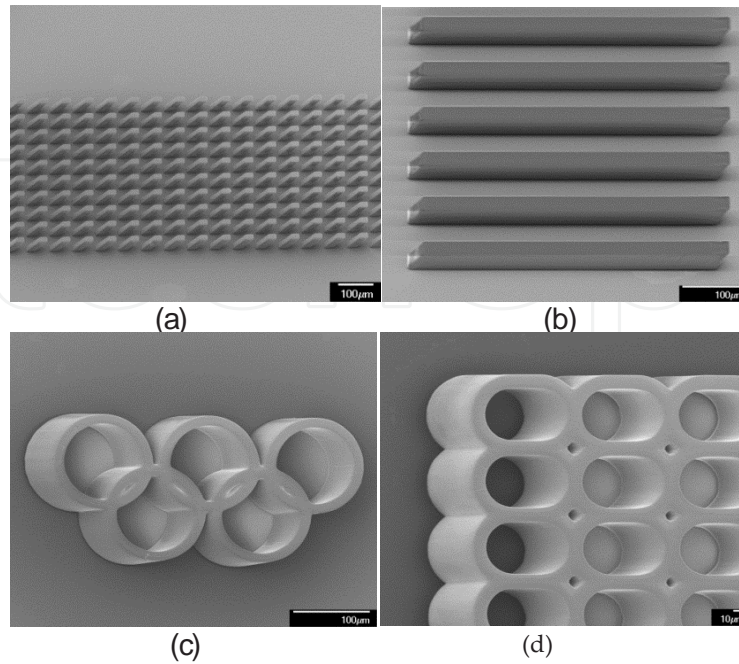


Figure 7. SEM images of the fabricated 3D inclined microstructures with 45° exposure angles.

The concept of utilizing the sample internal surface reflected exposing UV light to initiate cross-linking of the photoresist by increasing exposure times at a fixed UV light power (Campo & Arzt, 2008; Zhu et al., 2008) is given in Fig. 8. This is a simple yet efficient way to fabricate symmetric microstructures instead of twice exposures. The SEM images of the fabricated symmetric microstructures with 45° slanted surfaces on both sides are shown in Fig. 9 (Jiang et al., 2012b).

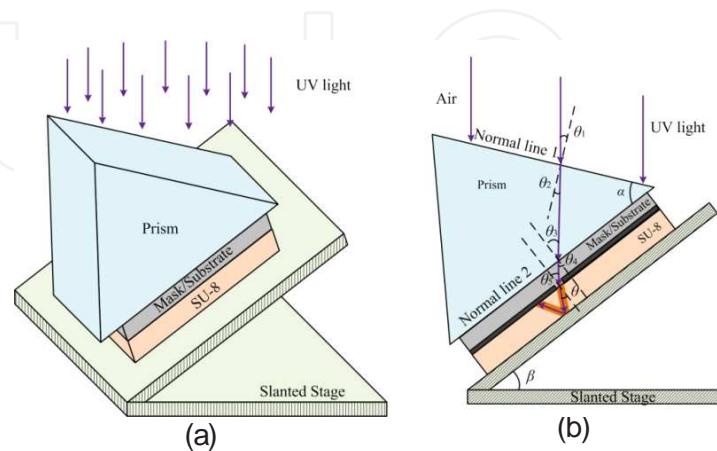


Figure 8. a) Schematic diagram of initiating cross-linking of the resin. (b) Schematic of cross-section view of the UV light path bending showing both incident and reflection exposures.

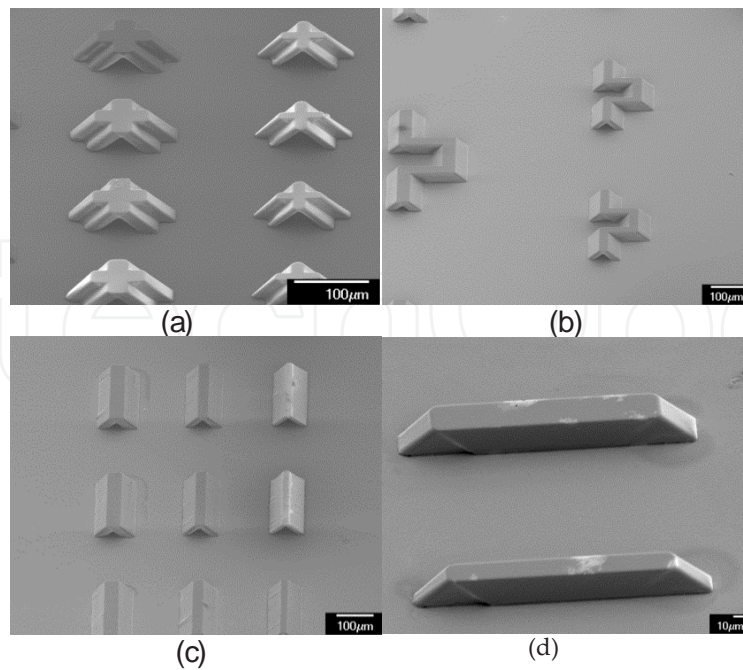


Figure 9. SEM images of the inclined structures with 45° exposure angles fabricated by internal reflected UV exposure beams.

2.2. Prism-assisted on-step UV lithography for multidirectional inclined structures

Besides the expansion of the exposure angle, the prism-assisted UV lithography is also attractive in one-step exposure fabrication of 3D structures with multi-directional inclined angles. The fabrication of V-cut structures with a right angle prism has been reported (Huang et al., 2008). A multi-surface optical prism of a polyhedron pyramid structure (a polyhedron pyramid prism) is introduced here to assist the fabrication of some particular microstructures as depicted in Fig. 10(a). Different side surfaces of the prism will simultaneously deflect UV light to different directions. Therefore, a set of slanted exposure beam columns will be formed by a set of refracted exposure beams from these side surfaces. It is thus possible to fabricate a complex multi-directional slanted structure in one step. Here, the slant stage angle β is set to be 0° . To illustrate this concept, we show the bending UV light paths from two side surfaces of the prism in Fig. 10(b).

A corner prism in Fig. 11 (a) was used in our experiment. It has a refractive index of 1.53 at 365 nm and a prism angle of 54.7° for all three side surfaces. The exposure angle θ in SU-8 caused by the refracted UV beams from each side-surface is 21° . When using a separated circular hole mask pattern, three slanted exposure beam columns are formed simultaneously by the refracted exposure beams from these three side surfaces. Thus, the exposure structure is an upside-down tripod structure. Fig. 11(b) and (c) present the fabricated upside-down tripod structures with different heights (Jiang et al., 2012a). Fig. 11(d) is the side view of the tripod structure when placing on its side which is dimensionally similar to that of Fig. 11(c).

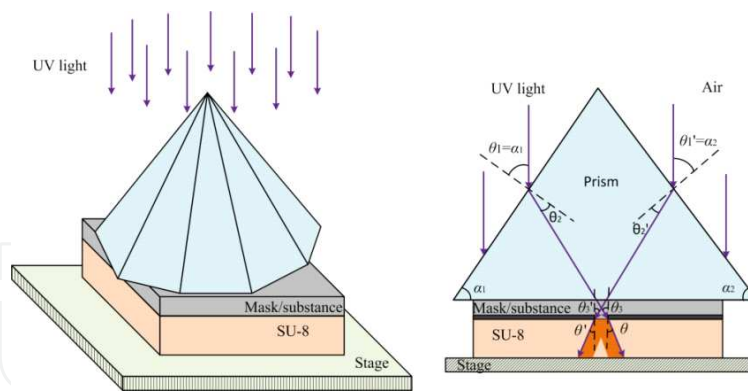


Figure 10. a) Schematic diagram of fabricating multi-directional structures using a polyhedron prism. (b) Schematic of a cross-sectional diagram showing the UV light paths.

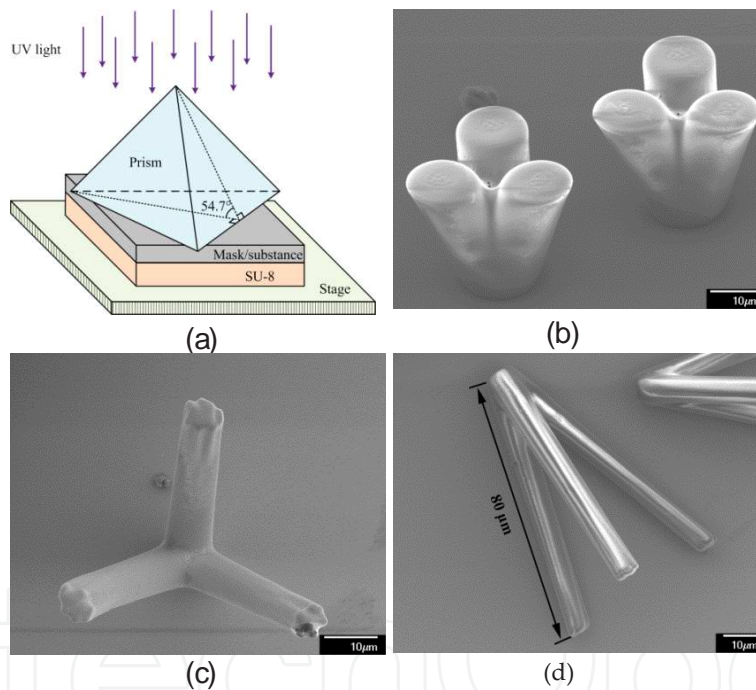


Figure 11. Fabrication of upside-down tripod structure by one-step exposure using a corner prism.

By arranging the basic upside-down tripod structures side by side, more complex 3D microstructures can be obtained. We use a mask pattern of an equilateral triangular lattice of circular holes in the experiment. If one base side of the prism is parallel to one side of the triangular lattice (see Fig. 12(a)), the nearest three upside-down tripod structures will intersect as shown in Fig. 12(b). If the prism is rotated in-plane by 90° , one base side of the prism will be vertical to one side of the triangular lattice (see Fig. 12(c)). The nearest three upside-down tripod structures will not intersect with each other and a new structure as illustrated in Fig. 12(d) is obtained.

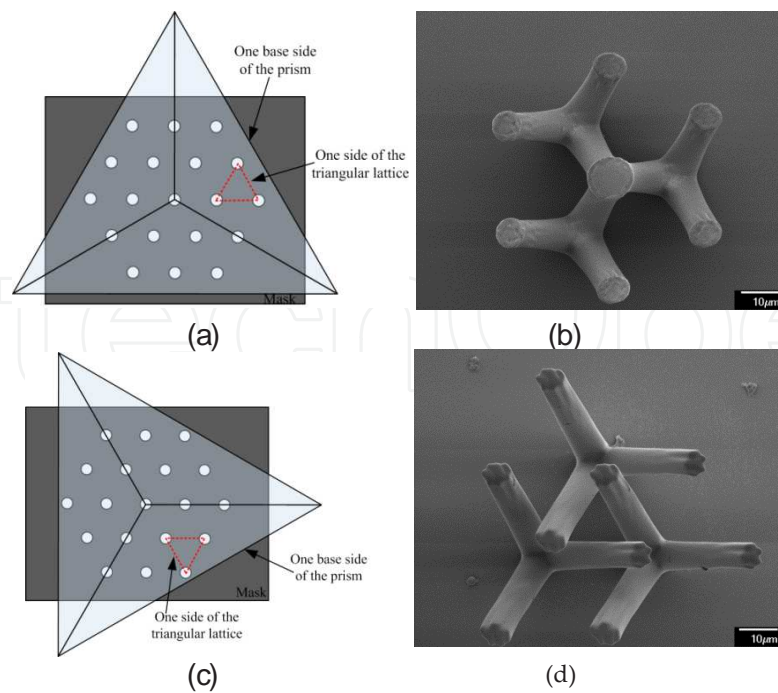


Figure 12. Two specific ways for the arrangement of the basic upside-down tripod structures.

With the setup in Fig. 12(a), the structure in Fig. 13(a) which owns a new layer with an equilateral triangular lattice of circular holes is formed when the height of the structure is $55\ \mu\text{m}$ and the side length of the triangular lattice on the mask is $36\ \mu\text{m}$. If we change the setup as shown in Fig. 12(c), the 3D mesh structure highlighted in Fig. 13(b) is realized when the side length of triangular lattice on the mask is $28\ \mu\text{m}$ and the height of the structure is $72\ \mu\text{m}$. This structure consists of three independent parts similar to that of Fig. 13(a). The three independent parts can be easily distinguished by following the color arrows indicated in Fig. 13(b), red arrows (the first part), blue arrows (the second part), and black arrows (the third part). Since this 3D mesh structure has three independent parts that are weaved closely together without intersecting, it may have a great strength and a greater flexibility. Therefore, this technique may be used to fabricate carbon fiber sheets with certain extensibility.

Fig. 13(c) and (d) presents a structure having one more layer than that of Fig. 12(a) which is achieved by adjusting the height of the structure to be $85\ \mu\text{m}$ and the side length of the triangular lattice to be $28\ \mu\text{m}$. The periodicity of this 3D microstructure in the vertical direction can be realized by increasing the height of the structures or decreasing the side length of the triangular lattice on the mask. This method may be applied to the fabrication of 3D photonic crystals at optical wavelengths if its size and periodicity can be further reduced.

If we replace the corner prism in Fig. 11(a) with a cone prism as illustrated in Fig. 14(a), circular symmetric 3D structures can be obtained. In the experiment, the cone prism (refractive index 1.53 at 365 nm) has a 60° prism angle. Since all refracted UV light beams from cone surface intersect at the center of the base plane, by position a circle hole mask pattern at the base center of the prism, the exposure pattern on the photoresist will show a horn structure. The fabricated

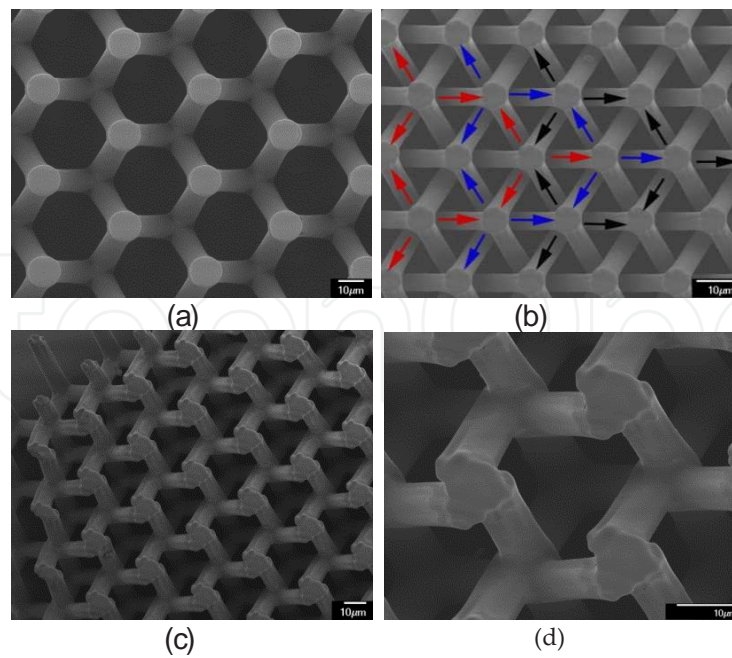


Figure 13. SEM images of the fabricated complex 3D microstructures using a corner prism.

horn structure is presented in Fig. 14(b) when using a mask with a 20 μm diameter circular hole pattern. The defects on the fabricated horn structure may be attributed to the misalignment between the center of circle pattern and the base center of prism and/or the imperfections of the cone prism.

If the circle hole mask pattern is not located at the center of the cone prism, the refracted UV light beams from cone surface to different directions will be asymmetric when passing through the circle hole mask pattern, so yielding asymmetric fan-shaped 3D structures. Fig. 14 (c) and (d) presents the asymmetric exposure patterns on the photoresist, when the circle holes mask pattern is 3 mm and 10 mm away from the base center of the prism, respectively. Because these holes are close to each other as a group but much farther away from the base center of the prism, these holes received similar asymmetric exposure and thus resulted in similar lithographic patterns. Clearly, different displacement from the base center of the prism will result in different asymmetric exposures.

When using a polyhedron pyramid prism for one-step UV lithographic fabrication of 3D multi-directional slanted structures, attention should be paid on the exposure dosage. There is certain beam energy lost as the UV light passes through the prism and interfaces. The exposure energy should be well controlled in the experiment. Fig. 15 shows the fabrication result of a similar structure as shown in Fig. 12(c) without enough exposure dosage. The nearest three upside-down tripod structures are intersecting, as we mentioned earlier. However, after photoresist developing, the inclined pillars cannot support the intersection resulting in the structural collapse. Over exposure may avoid the structural collapse but will introduce surface reflection exposure and structure size expansion that is also not desirable.

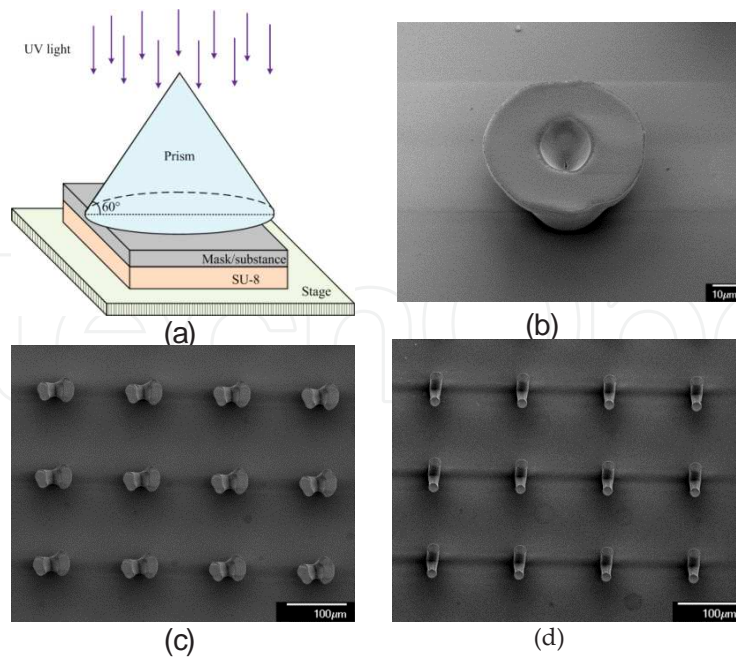


Figure 14. Fabrication of horn and fan-shaped structures by one-step exposure using a cone prism.

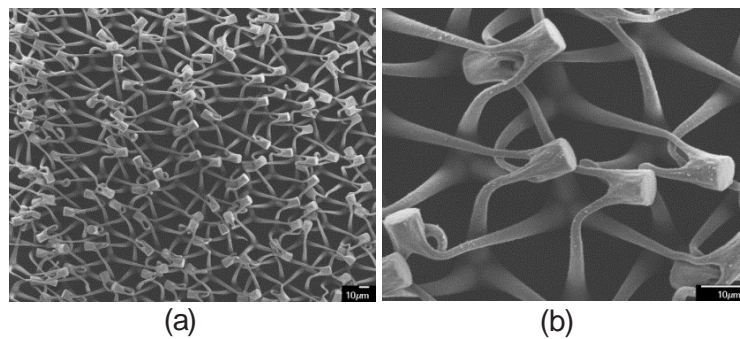


Figure 15. SEM images of the fabricated similar structure of Fig. 12(c) without enough exposure dosage with (b) as magnified view of a local portion of (a).

For multi-directional exposure, attention should also be paid on the effective exposure area of the prism, which also has a great influence on the formation of multi-directional slanted structures. Each side surface has its own projected exposure area (the projection of the side surface to the prism base), so the total effective exposure area means the common area of these projected exposure areas. Take a rotationally symmetric polyhedron pyramid prism as an example, the effective exposure area is determined by the slanted angle α of prism, the number of side surfaces n , and the circumradius r of the polygonal base. Fig. 16(a) shows the calculated results of effective exposure area (blue circles) and its percentage on the base area (red triangles) as a function of the number of side surfaces, at $\alpha = 60^\circ$ and $r = 25$ mm. The effective exposure area and its percentage decrease rapidly as the increase of the number of the side surfaces. Fig. 16(b) (blue solid line with $\alpha = 60^\circ$ and $n = 3$) shows that the effective exposure area can be enlarged by increasing the circumradius of the polygonal base when the number

of the side surfaces is fixed. We also found that the percentage of the effective exposure area is independent of the circumradius of the base, as indicated in Fig. 16(b) (red dashed line). Therefore the number of side surfaces and the circumradius of the base need to be reasonably selected in structural fabrication design.

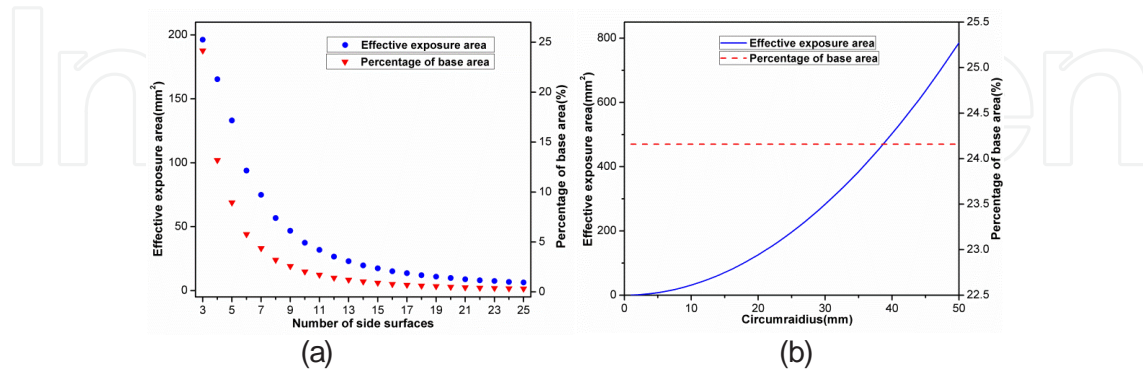


Figure 16. The effective exposure area and its percentage of base area (a) depend on the number of side surface and (b) depend on the circumradius of the base.

The prism-assisted inclined UV lithography is a flexible lithographic technique for the fabrication of 3D microstructures with different side surface angles. The one-step multi-directional exposure fabrication is attractive for fabricating complex 3D microstructures. The prism-assisted fabrication is also useful for the realization of periodic or quasi-periodic nanostructures through interference based holographic lithography discussed below.

3. Prism-assisted holographic lithography for nanostructures

The fabrication of periodic micro- and nano-structures can also be performed by a prism assisted holographic lithography technique. Holographic lithography has been used to fabricate photonic crystals (Yablonovitch, 1987; John, 1987) and metamaterial structures (Pendry et al., 1999; Smith et al., 2004; Soukoulis et al., 2007). Improvements in the HL for minimizing vibration sensitivity and simplifying fabrication process have been a constant and challenging issue. Besides holographic lithography (Berger et al., 1997; Shoji & Kawata, 2000; Campbell et al., 2000) that has demonstrated its suitability for fabrication of periodic micro- and nano-structures, there are other reported fabrication techniques like semiconductor lithography (Fleming & Lin, 1999) and chemical self-assembly (Zhou et al., 2000). The semiconductor lithography is a very expensive and slow process. It is also difficult to fabricate large area 3D structures. The chemical self-assembly technique is only capable of fabricating face-centered cubic structure with frequent appearance of defects. Holographic lithography is so far a low-cost promising technique in generating multiple interference exposure beams on photoresist for the realization of photonic crystal structures with defect-free micro- or nano-structures over a large area.

Holographic lithography based on the optical setup design can be classified as multiple beams single-exposure (Campbell et al., 2000; Wang et al., 2003; Ullal et al., 2004; Mao et al., 2005, 2006, 2007), two beams multi-exposure (Orlic et al., 2011), and Lloyd's mirror system (Choi & Kim, 2006; Jesson et al., 2007). The multiple beams single-exposure has the advantage of both simple fabrication process (one exposure) and tunable period and structure (1D, 2D and 3D, even quasi-crystals). However, this traditional method requires two independent steps: one is splitting the laser into multi-beams by beam splitters and then align the multi-beams to one point for interference and exposure (Campbell et al., 2000), which introduce significant adjustment complexity. The differences in the optical path lengths and angles among these beams are difficult to eliminate even with a highly skilled optical scientist. Furthermore, it requires very stable optical setup due to the vibration sensitivity of the HL system.

Recently, Wang et al. (2003) demonstrated a top-cut triangular prism (TCTP) that can be used to split one incident beam into four beams and automatically overlay them in the bottom of prism to form a 3D interference pattern in the light sensitive recording materials. They have significantly improved the stability of the optical setup and simplify the alignment of the multi-beams. Herein, we report our improved prism-assisted HL fabrication of micro- and nano-structures.

3.1. Theory of multi-beams interference

The 2D or 3D periodic patterns can be formed by interference of multiple coherent laser beams. In general, the interference equation is given by

$$I = \sum_i |E_i|^2 + \sum_{i,j} 2E_i E_j \cos \theta_{ij} \cos [(K_i - K_j)r + (\varphi_i - \varphi_j)]$$

where E_i , K_i and φ_i are the amplitude, wave vector and initial phase of the i th plane wave, and θ_{ij} is the angle of the polarizations between i,j th plane waves. For simplicity, we neglect the minor amplitude difference of different plane waves (assuming ideal equal amplitude beams), and treat all the initial phases as the same. We mainly discuss the wave vectors K_i s on how they affect the final pattern formation and add the influence of polarization to the pattern contrast.

It is well known that two beams of coherence light can form 1D periodic pattern, with periodic bright and dark stripes as shown in Fig. 17.

As we increase the number of interference beams, we define $G_k = K_i - K_j$ as the vector from K_j to K_i representing the reciprocal vectors of the periodic lattice structures. Once we determine the independent vectors G_k s, we also determine the lattice structure. The two beams have two wave vectors K_1 and K_2 , but only one independent $G_1 = K_1 - K_2$ (the vector $G_2 = K_2 - K_1 = -G_1$ is not independent). Thus, the interference pattern is 1D stripe. If the number of beams is more than 2, and $(G_k = K_i - K_j)$ s are all in the same plane but not parallel, we can generate 2D interference patterns. For example, with three symmetrical beams, the interference pattern is a hexagonal arrangement, as shown in Fig. 18(a). Four symmetrical beams would produce a

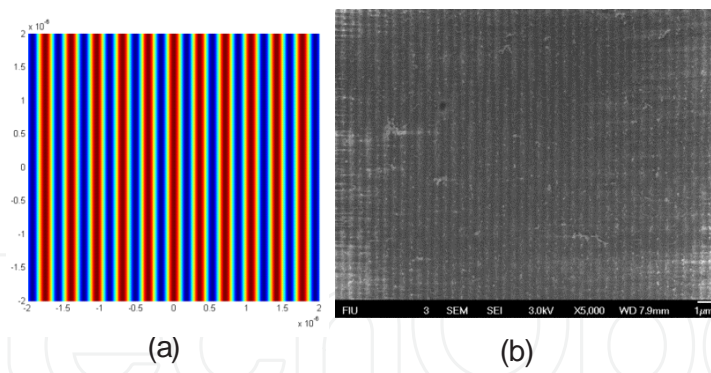


Figure 17. a) The simulated pattern of two beams interference in Matlab and (b) the observed exposed and developed pattern in photoresist under SEM.

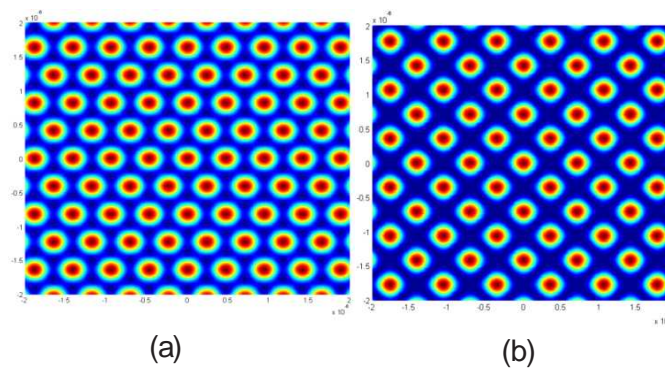


Figure 18. Simulated patterns come from the interference of three (a) and four (b) symmetrical beams.

square pattern shown in Fig. 18(b). These patterns can be realized in a photoresist after exposure and development.

These simple period patterns can be generated by laser or e-beam direct writing with relatively simple software control. The most attractive features of the HL is its capability in generating 3D and quasi-crystal patterns that are difficult by other pattern generating technique. Recently, Meisel *et al.* (2004) demonstrated the interference of umbrella-like four beams (this arrangement of beams will create 3 independent G_k s in 3D space) can form different crystal structures, such as simple cubic and face-centered cubic structure, simulated in Fig. 19.

Furthermore, these kinds of umbrella-like four beams can be easily realized by a top-cut triangular prism. Other groups have reported the use of prism-assist HL to create many different 3D structures (Wu *et al.*, 2004; Xu *et al.*, 2009; Park *et al.*, 2011). Meanwhile, Wang *et al.* (2003) firstly present 5-fold symmetry quasi-crystal by 5 symmetrical beams in half space, simulated in Fig. 20(a). Other symmetrical multi-beams (such as 5, 8, 10...) can yield novel quasi-crystal patterns, shown in Fig. 20(b). These structures have advantages over normal photonic crystals, like higher symmetry and lower refractive index requirement for photonic bandgap forming.

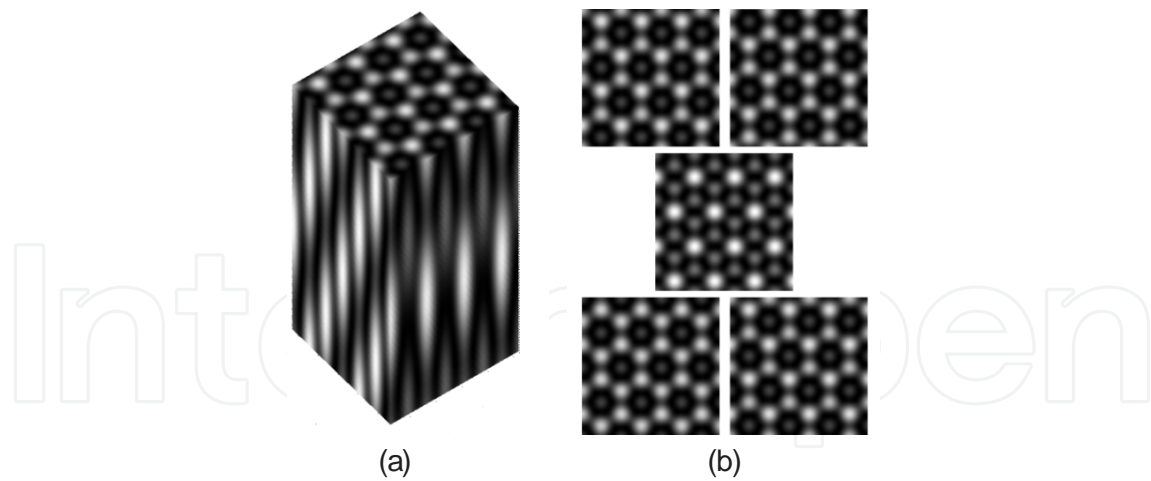


Figure 19. Simulated face-centered cubic structure (a) and the periodic changes of pattern on different X-Y planes (b).

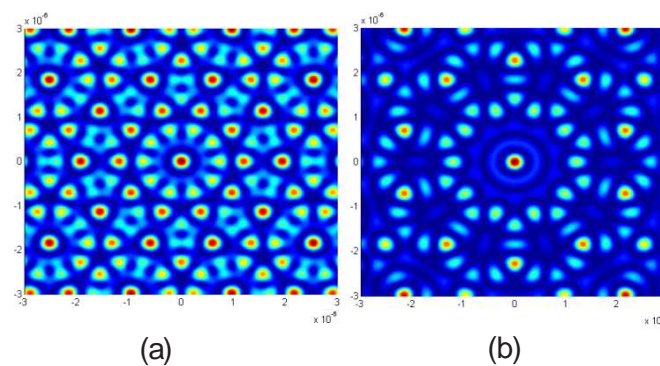


Figure 20. Simulated quasi-periodic pattern of five (a) and ten (b) symmetrical beams

The polarization states of these beams have significant effect to the interference patterns including the contrast and the pattern shape. Commonly, the intensity of cross terms $E_i E_j$ will be influenced by $\cos \theta_{ij}$, that will affect the contrast of final pattern. Su *et al.* (2003) investigated the relationship between the polarization and the contrast of the interference pattern, and detailed the optimum selection of polarizations for 3- and 4-beams. Furthermore, choosing special polarizations of different beams will significantly modify the final interference patterns, resulting in wood like 3D pattern (Park *et al.*, 2011) or U-shaped pattern (Yang *et al.*, 2008) for metamaterial.

We introduce a novel HL method to create photonic quasi-crystals by fewer beams. Naturally, the same number of beams may be chosen as the fold symmetry, namely 5 beams for 5-fold symmetry, 8 for 8, 10 for 10 and so on (Wang *et al.*, 2003). As the beam number is increased, the contrast of pattern will dramatically reduce due to the huge number of cross terms in the interference equation, making the fabrication very difficult or even impossible. Mao *et al.* (2006) demonstrated earlier that the design and fabrication of higher order photonic quasi-crystals with less number of laser beams. A quasi-periodic structure is regarded as a high dimensional periodic lattice projected onto a 3D space. There is an association between the high-dimen-

sional space and the number of independent reciprocal vectors G_k s. If a $(v+1)$ -dimensional space contains an N -fold symmetric periodic lattice, the smallest number v is given by the Euler totient function (Rabson et al. 1991)

$$v = \phi(N) = N \frac{(p_1 - 1)}{p_1} \frac{(p_2 - 1)}{p_2} \dots$$

where p_i s are distinct prime factors of N . Here we found that N -fold symmetry quasi-crystal does not need the same number of beams. For example, an 8-fold symmetry with the prime factor of 2, we have $v + 1 = 8(1 - 1/2) + 1 = 5$, that means we just need 5 beams to form an 8-fold photonic quasi-crystal. Furthermore, 10- and 12-fold symmetry quasi-crystals also only need 5 beams. The arrangement of interference beams and simulation of the interference pattern are illustrated in Fig. 21.

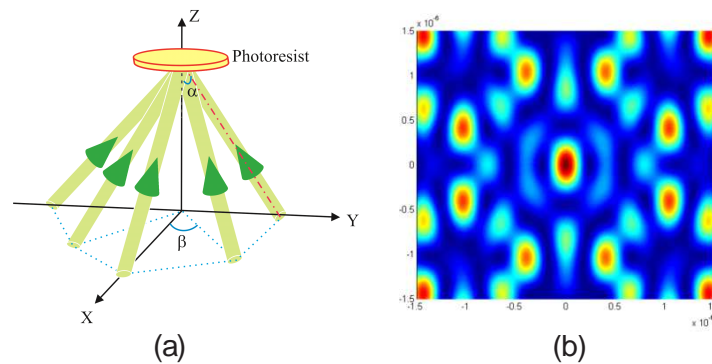


Figure 21. a) The arrangement of 5 beams in $1/4$ space for eight fold symmetrical interference pattern, where $\alpha = 26.3^\circ$ and $\beta = 45^\circ$. (b) Simulated interference pattern of the special five beams.

3.2. Fabrication of micro- and nano-structures by holographic lithography

3.2.1. Specially designed prism

Generally speaking, the geometry structure of the five coherent beams as shown in Fig. 21 can be configured by beam splitters and mirrors. But this type of conventional setup is subjected to critical alignment and sensitivity to slight positional deviation and minor phase shift, which lead to instability of final interference pattern. The specially configured prism of Fig. 22 can directly split an incident laser beam into five laser beams almost without relative phase shift and difference in optical path length, and overlap in the bottom of the prism. Figure 22(a) illustrates our designed prism with a 45° angle between the side surface and the bottom. For refractive index $n=1.51$, the emergent laser beams from bottom will illuminate the photoresist with an angle of 26.3° . The specially configured prism consists of two parts – cone and cylinder. The diameter of the bottom is 25.4 mm and the heights of the cone and cylinder are 12.7 mm and 5 mm, respectively.

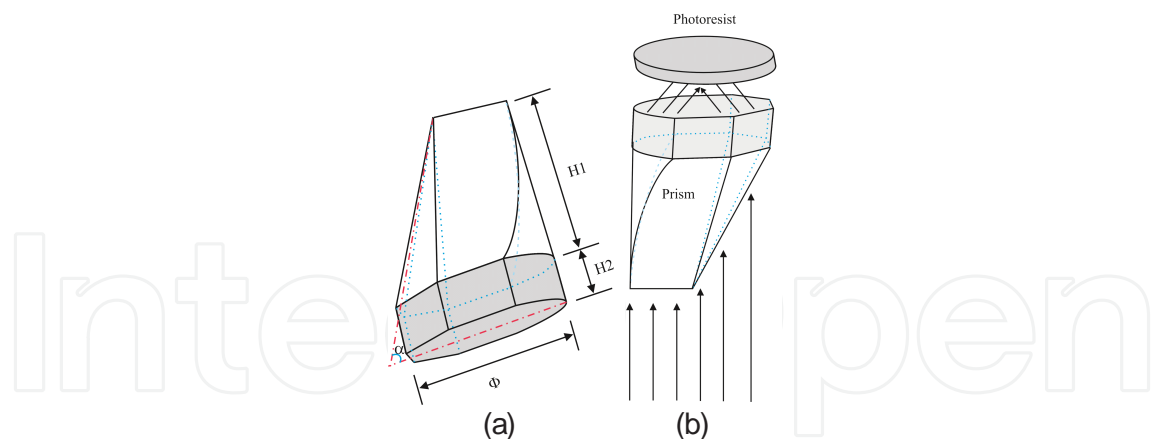


Figure 22. a) Specially configured prism for holographic eight-fold photonic quasi-crystal with only five continuous surfaces out of symmetrical eight side surfaces. Here $\Phi = 25.4$ mm, $H_1 = 12.7$ mm, $H_2 = 5$ mm, and $\alpha = 45^\circ$. (b) Optical setup showing incident laser beam, the prism, and the photoresist.

A unique feature of this specially designed prism is that it has only five continuous surfaces out of symmetrical eight surfaces of the prism. Compared with eight beams from eight side surfaces to form eight-fold symmetric quasi-periodicity, this design of using only five continuous surfaces will dramatically improve the contrast of interference.

3.2.2. Prism-assisted fabrication of 8-fold quasi-crystals with 5 beams

In experiments, the photoresist solution was prepared by mixing 1.0 wt% of a photoinitiator, Cyclopentadienyl(fluorene)iron(II) hexafluorophosphate (Aldrich), in an SU-8 solution (Micro-Chem, SU-8 3010 diluted by SU-8 thinner (3:2)), that is sensitive to green light including the 532 nm wavelength. This photoresist was spin coated (4000 rpm for 30s) on glass plates and pre-baked at $\sim 91^\circ\text{C}$ for about 1 h. A 532 nm linearly polarized laser beam from a diode pumped solid state laser (Crystalaser) with output power of 60 mW was expanded by spatial filter and collimated by a collimation lens. The expanded laser beam was incident from the top side of the prism and recombined at the bottom of the prism, or the plane of photoresist. After about 10s of exposure, the sample was post-baked at $\sim 93^\circ\text{C}$ for about 1 h to complete polymerization and developed in SU-8 developer (Micro-Chem) for 1 h, followed by rinse in isopropanol. The surface morphologies were investigated by scanning electron microscopy (SEM; JEOL JSM-7000F).

Fig. 23 exhibits four SEM images of holographic eight-fold quasi-crystals. For an appropriate exposure time, an obtained eight-fold quasi-crystal with clear features is shown in Fig. 23(a) and (b). Fig. 23(b) is a magnified image of the same structure of (a), showing more details. When over exposed, the dots will connect with each other as shown in Fig. 23(c) and (d), due to the degree of over exposures, but still revealing eight-fold symmetry. Therefore, eight-fold quasi-crystals can be fabricated by prism assist five beam single-exposure holographic lithography instead of usual eight beams. Additionally, if only use three continuous surfaces, we can get some novel patterns, such as bias short line hexagonal arrangement, as shown in Fig. 24.

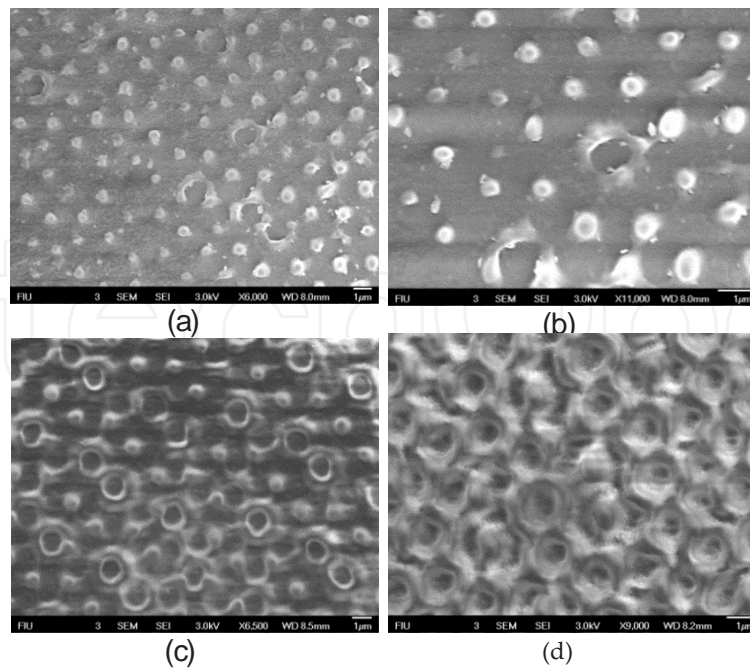


Figure 23. a) After an appropriate exposure time, we get clear picture of eight fold quasi-periodic pattern and (b) its local magnified picture with more details. (c) and (d) show the quasi-periodic patterns realized by slightly and highly over exposures, respectively.

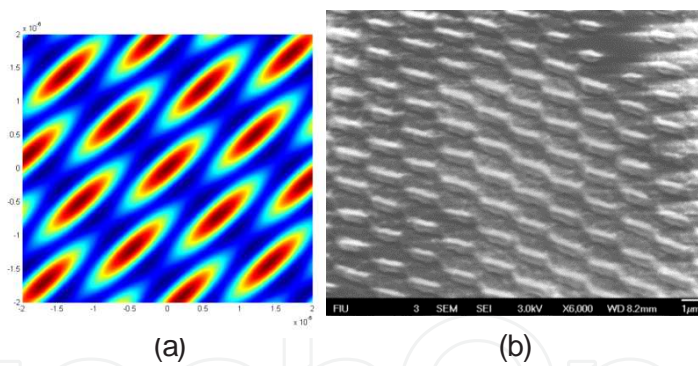


Figure 24. Simulation (a) and SEM picture (b) of three continuous side surfaces interference of this special prism.

4. Application of micro- and nano-structures

Many practical applications of 3D micro- and nano-structures have been reported, such as V-grooves for fiber holder (Ling & Lian, 2007), mesh structures for microfilter (Sato et al., 2004), inclined surfaces for the optical pick-up head (Huang et al., 2004), pyramid array for optical display (Yoon et al., 2006; Shieh et al., 2005), some complex microstructures for micromixer (Baek et al., 2011; Sato et al., 2006) and drug delivery (Han et al., 2007; Yoon et al., 2011), and periodic array for photonic crystal. In this section, we will demonstrate our exploitation of

micro- and nano-structures applications on 45° inclined mirrors and microfilter system, fabricated by the prism-assisted photolithography.

4.1. 45° inclined mirrors for card-to-backplane optical interconnect

Optical interconnects have been extensively researched for high-speed computing systems because of the speed limitations and drawbacks of electrical routing on boards (Doany et al., 2009). Polymer waveguides with 45° inclined mirrors are important components in optical interconnect (Lee et al., 2009; Wang et al., 2005; Wang et al., 2008; Glebov et al., 2005). We fabricated 45° inclined mirror structures in the master photoresist by prism-assisted UV lithography (Jiang et al., 2012c). Sample surface reflected UV light was utilized to eliminate undercut structures and to accomplish the inclined mirror surfaces on both ends of the straight waveguide segments by one-step UV exposure, as shown in Fig. 25. High quality microfluidic channels are then transferred to a PDMS mold. The vacuum assisted microfluidic soft lithography fabrication (Flores et al., 2008) using UV curable core waveguide resin yield the polymer waveguides with 45° inclined surfaces. Fig. 26 illustrates the SEM image of imprinted polymer waveguide before aluminum local coating. After aluminum local coating on the slanted surfaces followed by lower index cladding layer over coating it results in embedded polymer waveguides for optical interconnection. Surface normal optical coupling from the waveguide has been demonstrated supporting the card-to-backplane optical interconnects.

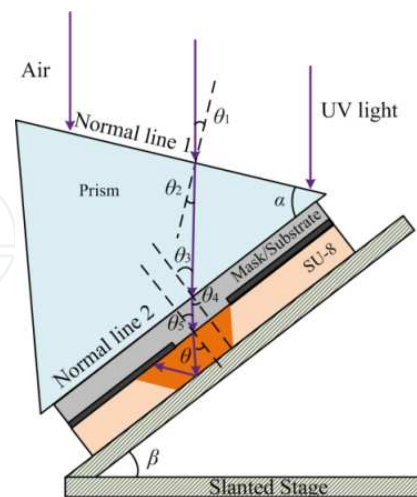


Figure 25. Schematic diagram of fabricating 45° inclined mirror surfaces on both ends of the straight waveguide.

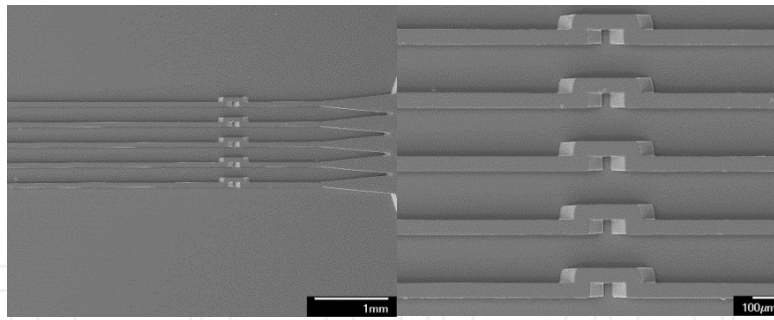


Figure 26. SEM images of imprinted polymer waveguide before aluminum local coating.

4.2. Mesh structures for microfilter system

A right angle prism (refractive index 1.53 at 365 nm) was utilized for the one-step fabrication of micromesh structures in our experiment, as shown in Fig. 27. Fig. 28 (a) and (c) illustrates the fabricated micromesh structures with different mesh size of 20 μm and 10 μm respectively, which can be easily found from their enlarge parts in Fig. 28(b) and (d). The mesh size can be easily adjusted by changing the distance between rectangles on photomask. We can increase number of the mesh layers by enlarging the height of structure or decreasing the period of the rectangle array. After the fabrication of the micromesh structures, a PDMS mode with microfluidic channel on the bottom is placed on the top of the mesh structures for the microfilter system. This microfluidic channel should own the same width and height as these mesh structures.

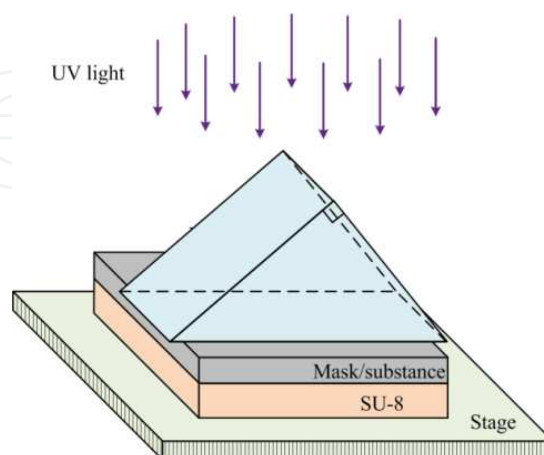


Figure 27. Schematic diagram of fabrication of mesh structures by a right angle prism.

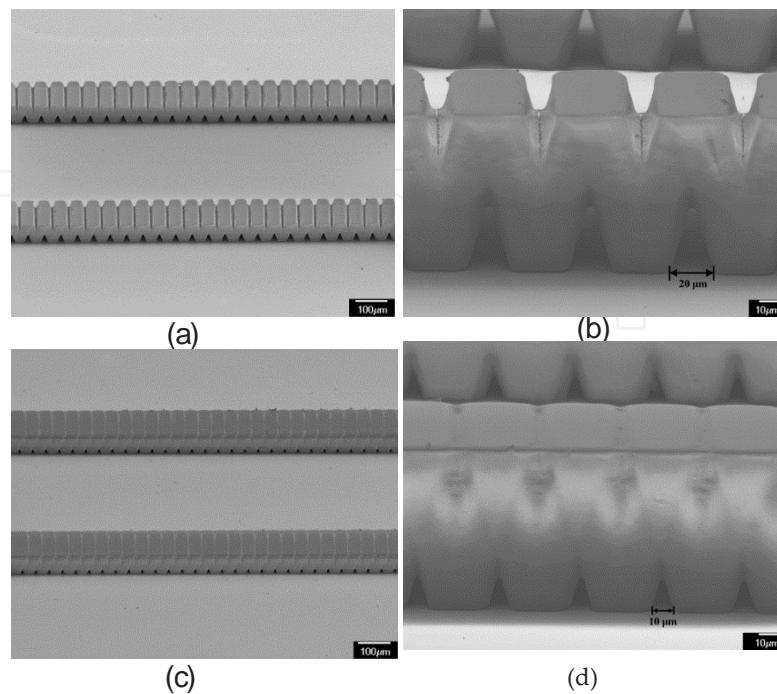


Figure 28. SEM images of micromesh structures with different mesh size.

5. Conclusion

In this chapter, the prism-assisted UV lithography and holographic lithography are introduced for the fabrication of 3D micro- and nano-structures. For prism-assisted inclined UV lithography, a prism is used as a refractor to deflect the incident UV light and control the exposure beams directions in the resist. Slanted structures with exposure angles ranging from 0° to 60° can be easily achieved. The sample internal surface reflection of the exposing UV light can be further utilized for the fabrication of symmetric structures. The fabrication of multi-directional slanted structures can be simplified by one-step UV exposure using a prism with multi-directional side surfaces. For holographic lithography, a prism is used to simplify the process in conventional HL and at the same time improve the system stability. The prism-assisted HL is advantageous for realization of periodic sub-micro and nano structures over a large area. Some practical applications of our fabricated structures, such as 45° inclined mirrors and microfilter system, are also discussed. With setup simplicity, cost effectiveness and fabrication flexibility, the prism-assisted UV and holographic lithography techniques should aid in the fabrication of various 3D micro- and nano-structures.

Acknowledgements

The work is sponsored in part by the National Science Foundation. The authors thank Hui Lu, Sarfaraz Baig, and Bing Li for helpful discussions.

Author details

Guomin Jiang, Kai Shen and Michael R. Wang

University of Miami, USA

References

- [1] Baek, S, & Song, S. A. (2011). A one-step photolithography method for fabrication of a staggered herringbone mixer using inclined UV lithography. *J. Micromech. Microeng.* 21 077001
- [2] Berger, V, Gauthier-lafaye, O, & Costard, E. (1997). Photonic band gaps and holography. *J. Appl. Phys.* , 82, 60-64.
- [3] Beuret, C, Racine, G. A, Gobet, J, Luthier, R, & De Rooij, N. F. (1994). Microfabrication of 3D multidirectional inclined structures by UV lithography and electroplating. *Proc. IEEE Int. Conf. on Micro Electro Mechanical Syst. (MEMS 1994)* , 81-85.
- [4] Campbell, M, Sharp, D. N, Harrison, M. T, Denning, R. G, & Turberfield, A. J. (2000). Fabrication of photonic crystals for the visible spectrum of holographic lithography. *Nature*, 404, 53-56.
- [5] Campo, A. d, & Arzt, E. (2008). Fabrication approaches for generating complex micro- and nanopatterns on polymeric surfaces. *Chem. Rev.* , 108-911.
- [6] Campo, A. d, & Greiner, C. (2007). SU-8 a photoresist for high-aspect-ratio and 3D submicron lithography. *J. Micromech. Microeng.* , 17, R81-R95.
- [7] Choi, C. -H, & Kim, C. J. (2006). Fabrication of dense array of tall nanostructures over a large sample area with sidewall profile and tip sharpness control. *Nanotechnol.* , 17, 5326-5333.
- [8] Doany, F. E, Schow, C. L, Baks, C. W, Kuchta, D. M, Pepeljugoski, P, Schares, L, Budd, R, Libsch, F, Dangel, R, Horst, F, Offrein, B. J, & Kash, J. A. (2009). 160 Gb/s Bidir- Lithography ectional Polymer-Waveguide Board-Level Optical Interconnects Using CMOS-Based Transceivers. *IEEE Trans. Adv. Package* , 32, 345-359.

- [9] Doua, X, Wangb, X, Huanga, H, Lina, X, Dinga, D, Pana, D. Z, & Chen, R. T. (2010). Polymeric waveguides with embedded micromirrors formed by Metallic Hard Mold. *Opt. Express* , 18, 378-385.
- [10] Fleming, J. G, & Lin, S. -Y. (1999). Three-dimensional photonic crystal with a stop band from 1.35 to 1.95 μm . *Opt. Lett.* , 24, 49-51.
- [11] Flores, A, Song, S, Baig, S, & Wang, M. R. (2008). Vacuum-assisted microfluidic technique for fabrication of guided wave devices. *IEEE Photon. Technol. Lett.* , 20, 1246-1248.
- [12] Glebov, A. L, Roman, J, Lee, M. G, & Yokouchi, K. (2005). Optical interconnect modules with fully integrated reflector mirrors. *IEEE Photon. Technol. Lett.* , 17, 13 1540-1542.
- [13] Han, M, Hyun, D. -H, Park, H. -H, Lee, S. S, Kim, C. H, & Kim, C. G. (2007). A novel fabrication process for out-of-plane microneedle sheets of biocompatible polymer. *J. Micromech. Microeng.* , 17, 1184-1191.
- [14] Han, M, Lee, W, Lee, S, -K, & Lee, S. S. (2004). 3D microfabrication with inclined/rotated UV lithography. *Sensors Actuators A* , 111, 14-20.
- [15] Huang, Y, -J, Chang, T. -L, Chou, H. -P, & Lin, C. -H. (2008). A novel fabrication Method for forming inclined groove-based microstructures using optical elements. *Japanese Journal of Applied Physics* , 47, 5287-5290.
- [16] Hung, K. Y, Hu, H. T, & Tseng, F. G. (2004). Application of 3D glycerol-compensated inclined-exposure technology to an integrated optical pick-up head. *J. Micromech. Microeng.* , 14, 975-983.
- [17] Jesson, D. E, Pavlov, K. M, Morgan, M. J, & Usher, B. F. (2007). Imaging surface topography using Lloyd's mirror in photoemission electron microscopy. *Phys. Rev. Lett.* 99, 016103
- [18] Jiang, G, Baig, S, & Wang, M. R. (2012). 3D microstructures fabricated by prism assisted inclined UV lithography. *Proc. SPIE 8249 82490L*
- [19] Jiang, G, Baig, S, & Wang, M. R. (2012). Prism-Assisted Inclined UV Lithography for 3D Microstructures Fabrication. *J. Micromech. Microeng.* 22 085022
- [20] Jiang, G, Baig, S, & Wang, M. R. (2012). Soft Lithography Fabricated Polymer Waveguides with 45° Inclined Mirrors for Card-to-Backplane Optical Interconnects. *Proc. SPIE*, 8267, Jan. 24,
- [21] John, S. (1987). Strong localization of photons in certain disordered dielectric superlattices. *Phys. Rev. Lett.* , 58, 2486-2489.
- [22] Kang, W. -J, Rabe, E, Kopetz, S, & Neyer, A. (2006). Novel exposure methods based on reflection and refraction effects in the field of SU-8 lithography. *J. Micromech. Microeng.* , 16, 821-831.

- [23] Lee, W, Hwang, S. H, Lim, J. W, & Rho, B. S. (2009). Polymeric Waveguide Film with Embedded Mirror for Multilayer Optical Circuits. *Photon. Technol. Lett.* , 21, 12-14.
- [24] Ling, Z, & Lian, K. (2007). SU-8 3D microoptic components fabricated by inclined UV lithography in water. *Microsyst. Technol.* , 13, 245-251.
- [25] Mao, W. D, Liang, G. Q, Pu, Y. Y, Wang, H. Z, & Zeng, Z. H. (2007). Complicated three-dimensional photonic crystals fabricated by holographic lithography *Appl. Phys. Lett.* 91, 261911
- [26] Mao, W. D, Liang, G. Q, Zou, H, & Wang, H. Z. (2006). Controllable fabrication of two-dimensional compound photonic crystals by single-exposure holographic lithography. *Opt. Lett.* , 31, 1708-1710.
- [27] Mao, W. D, Liang, G. Q, Zou, H, Wang, H. Z, Zhang, R, & Zeng, Z. H. (2006). Design and fabrication of two-dimensional holographic photonic quasi crystals with high-order symmetries. *J. Opt. Soc. Am. B* , 23, 2046-2050.
- [28] Mao, W. D, Wathuthanthri, I, & Choi, C. -H. (2011). Tunable two-mirror interference lithography system for wafer-scale nanopatterning. *Opt. Lett.* , 36, 3176-3178.
- [29] Mao, W. D, Zhong, Y. C, Dong, J. W, & Wang, H. Z. (2005). Crystallography of two dimensional photonic lattices formed by holography of three noncoplanar beams. *J. Opt. Soc. Am. B* , 22, 1085-1091.
- [30] Meisel, D. C, Wegener, M, & Busch, K. (2004). Three-dimensional photonic crystals by holographic lithography using the umbrella configuration: Symmetries and complete photonic band gaps. *Phys. Rev. B* 70, 165104
- [31] Orlic, S, Müller, C, & Schlösser, A. (2011). All-optical fabrication of three-dimensional photonic crystals in photopolymers by multiplex-exposure holographic recording. *Appl. Phys. Lett.* 99, 131105
- [32] Park, S, Miyake, M, Yang, S, & Braun, P. (2011). Cu₂O Inverse Woodpile Photonic Crystals by Prism Holographic Lithography and Electrodeposition. *Adv. Mater.* , 24, 2749-2752.
- [33] Pendry, J. B, Holden, A. J, Robbins, D. J, & Stewart, W. J. (1999). Magnetism from conductors and enhanced nonlinear phenomena. *IEEE Trans. Microwave Theory Tech.* , 47, 2075-2084.
- [34] Rabson, D. A, Mermin, N. D, Rokhsar, D. S, & Wright, D. C. (1991). The space groups of axial crystals and quasicrystals. *Rev. Mod. Phys.* , 63, 699-733.
- [35] Sato, H, Kakinuma, T, Go, J. S, & Shoji, S. (2004). In-channel 3-D micromesh structures using maskless multi-angle exposures and their microfilter application. *Sensors Actuators A* , 111, 87-92.

- [36] Sato, H, Yagyu, D, Ito, S, & Shoji, S. (2006). Improved inclined multi-lithography using water as exposure medium and its 3D mixing microchannel application. *Sensors Actuators A* , 128, 183-190.
- [37] Shieh, H. -P. D, Huang, Y. -P, & Chien K. -W. (2005). Micro-optics for Liquid Crystal Displays Applications. *IEEE/OSA journal of display technology* , 1, 62-76.
- [38] Shoji, S, & Kawata, S. (2000). Photofabrication of three-dimensional photonic crystals by multibeam laser interference into a photopolymerizable resin. *Appl. Phys. Lett.* 11 76, 2668-2670.
- [39] Smith, D. R, Pendry, J. B, & Wiltshire, M. C. K. (2004). Metamaterials and negative refractive index. *Science* , 305, 788-792.
- [40] Soukoulis, C. M, Linden, S, & Wegener, M. (2007). Physics: negative refractive index at optical wavelengths. *Science* , 315, 47-49.
- [41] Su, H. M, Zhong, Y. C, Wang, X, Zheng, X. G, Xu, J. F, & Wang, H. Z. (2003). Effects of polarization on laser holography for microstructure fabrication. *Phys. Rev. E* 67, 056619
- [42] Ullal, C. K, Maldovan, M, Thomas, E. L, Chen, G, Han, Y. J, & Yang, S. (2004). Photonic crystals through holographic lithography: Simple cubic, diamond-like, and gyroid-like structures. *Appl. Phys. Lett.* , 84, 5434-5436.
- [43] Wang, G. P, Tan, C, Yi, Y, & Shan, H. (2003). Holography for one-step fabrication of three-dimensional metallodielectric photonic crystals with a single continuous wavelength laser beam. *J. Mod. Opt.* , 50, 2155-2161.
- [44] Wang, L, Wang, X, Jiang, W, Choi, J, Bi, H, & Chen, R. T. (2005). 45° polymer-based total internal reflection coupling mirrors for fully embedded intraboard guided wave optical interconnects. *Appl. Phys.*, 87, 141110
- [45] Wang, X, Jiang, W, Wang, L, Bi, H, & Chen, R. T. (2008). Fully embedded board-level optical interconnects from waveguide fabrication to devices integration. *J. Lightw. Technol.* , 26, 243-250.
- [46] Wang, X, Ng, C. Y, Tam, W. Y, Chan, C. T, & Sheng, P. (2003). Large-area two-dimensional mesoscale quasi-crystals. *Adv. Mater.* , 15, 1526-1528.
- [47] Wang, X, Xu, J. F, Su, H. M, Zeng, Z. H, Chen, Y. L, Wang, H. Z, Pang, Y. K, & Tam, W. Y. (2003). Three-dimensional photonic crystals fabricated by visible light holographic lithography. *Appl. Phys. Lett.* , 82, 2212-2214.
- [48] Wu, L, Zhong, Y, Chan, C. T, Wong, K. S, & Wang, G. P. (2005). Fabrication of large area two- and three-dimensional polymer photonic crystals using single refracting prism holographic lithography. *Appl. Phys. Lett.* 86, 241102

- [49] Xu, D, Chen, K. P, Harb, A, Rodriguez, D, Lozano, K, & Lin, Y. K. (2009). Phase tunable holographic fabrication for three-dimensional photonic crystal templates by using a single optical element. *Appl. Phys. Lett.* 94, 231116
- [50] Yablonovitch, E. (1987). Inhibited Spontaneous Emission in Solid-State Physics and Electronics. *Phys. Rev. Lett.* , 58, 2059-2062.
- [51] Yang, Y, Li, Q, & Wang, G. P. (2008). Design and fabrication of diverse metamaterial structures by holographic lithography. *Optics Express* 16, 11275-11280.
- [52] Yoon, Y. -K, Park, J. -H, & Allen, M. G. (2006) Multidirectional UV lithography for complex 3-D MEMS structures. *IEEE J. Microelectromech. Syst.* 15, 1121-1130.
- [53] Yoon, Y. -K, Park, J. -H, Lee, J. -W, Prausnitz, M. R, & Allen, M. G. (2011). A thermal microjet system with tapered micronozzles fabricated by inclined UV lithography for transdermal drug delivery. *J. Micromech. Microeng.* 21 025014
- [54] Zhou, J, Zhou, Y, Ng, S. L, Zhang, H. X, Que, W. X, Lam, Y. L, Chan, Y. C, & Kam, C. H. (2000). Three-dimensional photonic band gap structure of a polymer-metal composite. *Appl. Phys. Lett.* 76, 3337
- [55] Zhu, Z, Zhou, Z. -F, Huang, Q. -A, & Li, W. -H. (2008). Modeling simulation and experimental verification of inclined UV lithography for SU-8 negative thick photoresists. *J. Micromech. Microeng.* 18 125017